
Improved Convex Decomposition with Ensembling and Boolean Primitives

Vaibhav Vavilala
UIUC

Florian Kluger
Leibniz Universität Hannover

Seemandhar Jain
UIUC

Bodo Rosenhahn
Leibniz Universität Hannover

David Forsyth
UIUC

Abstract

Describing a scene in terms of primitives – geometrically simple shapes that offer a parsimonious but accurate abstraction of structure – is an established vision problem. This is a good model of a difficult fitting problem: different scenes require different numbers of primitives and primitives interact strongly, but any proposed solution can be evaluated at inference time. The state of the art method involves a learned regression procedure to predict a start point consisting of a fixed number of primitives, followed by a descent method to refine the geometry and remove redundant primitives. Methods are evaluated by accuracy in depth and normal prediction and in scene segmentation. This paper shows that very significant improvements in accuracy can be obtained by (a) incorporating a small number of *negative* primitives and (b) ensembling over a number of different regression procedures. Ensembling is by refining each predicted start point, then choosing the best by fitting loss. Extensive experiments on a standard dataset confirm that negative primitives are useful in a large fraction of images, and that our refine-then-choose strategy outperforms choose-then-refine, confirming that the fitting problem is very difficult.

1 Introduction

Geometric representations of scenes and objects as *primitives* – simple geometries that expose structure while suppressing detail – should allow simpler, more general reasoning. For example, it is easier to plan moving a cuboid through a stylized free space than it is to plan moving a particular chair through a particular living room; as another example, an effective primitive representation should simplify selecting and manipulating objects in scenes (and so image-based scene editing [53]). But obtaining primitive representations that abstract usefully and accurately has been hard (review Sec. 2).

There are two main types of method. A **descent method** chooses primitives for a given geometry by minimizing a cost function. Important obstacles include: different geometries require different numbers of primitives; the choice of primitive appears to be important in ways that are opaque; the fitting problem appears to have large numbers of local minima; and finding a good start point is difficult. In particular, incremental fitting procedures are often defeated by interactions between primitives. A **regression method** uses a learned predictor to map geometry to primitives and their parameters. These methods can pool examples to avoid local minima, but may not get the best prediction for a given input.

The SOTA method [52] for parsing indoor scenes uses a regression method to predict a start point consisting of a fixed set of primitives. An important feature of this class of problem is that, *at run time*, one can evaluate a predicted solution efficiently and accurately. The start point is then

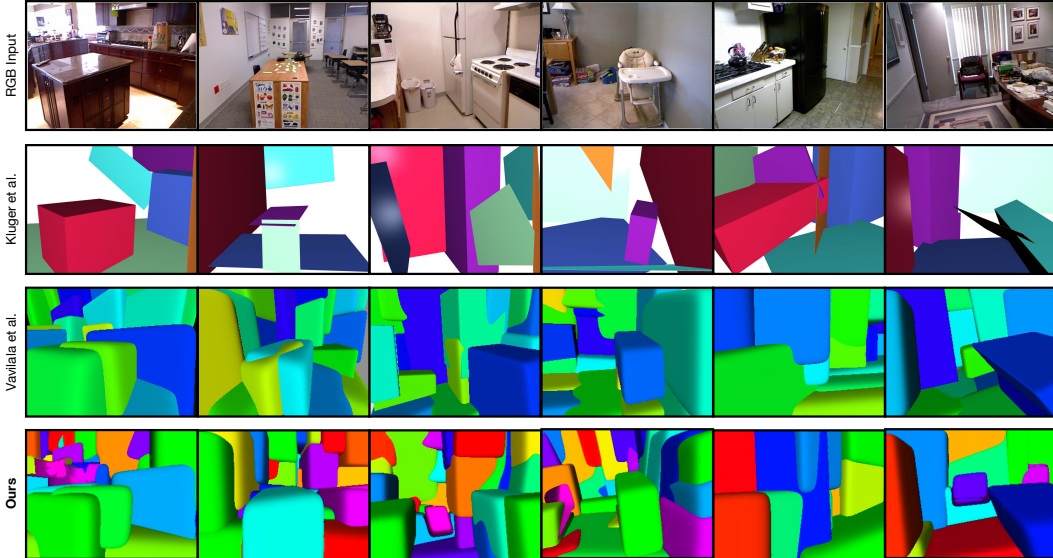


Figure 1: We present a method that advances the SOTA for primitive decomposition of indoor scenes, by using ensembling and boolean primitives. We present qualitative comparison with prior work here. In the fourth column, notice how a negative primitive helps explain free space on the bottom left; in the last column, notice how a negative primitive helps represent the chair in the center.

polished using a descent method, applied to a fitting loss that compares the prediction with depth and segmentation maps predicted by a suitable pretrained network, with backward selection to remove redundant primitives. Finally, evaluation is by comparing the primitive geometry to reference depth, normal and segmentation.

This paper shows two procedures that yield significant (over 30% relative error) improvements in accuracy. First, we allow a small number of *negative* primitives in the sense of constructive solid geometry (CSG). Second, we show that an appropriately constructed ensembling method produces very strong improvements in accuracy.

For **negative primitives**, the predicted geometry is the set difference between the union of positive primitives and the union of negative primitives. As our ablation experiments show, this significantly expands the geometries we can encode and significantly complicates the fitting problem. On their own, negative primitives produce small improvements in accuracy. With **ensembling** we obtain significant improvements in accuracy. We ensemble by using multiple predictors, each trained to predict a start point with a different number of primitives; some predictors use only positive primitives, others use both positive and negative primitives. Each predicted start point is then polished by minimising a fitting loss, and the best resulting set of primitives by fitting loss is reported. This polish-then-choose strategy yields very strong improvements in accuracy. Notably, for some scenes only positive primitives are used, whereas for others both positive and negative primitives are used.

Our contributions are:

1. We believe our method is the only one that can fit CSG with a set differencing operator to indoor scenes.
2. Our ensembling method has a novel structure that results in large improvements in accuracy.
3. Our primitive decomposition method for indoor scenes is an effective procedure that substantially outperforms SOTA on established metrics on the benchmark NYUv2 dataset.

2 Related Work

Primitives date to the origins of computer vision. Roberts worked with blocks [43]; Binford with generalized cylinders [4]; Biederman with geons [3]. Ideally, complex objects might be handled with

simple primitives [6], each primitive is a semantic part [3, 4, 51]. Primitives can be recovered from image data [36, 44], and allow simplified geometric reasoning [39].

For individual objects, neural methods could predict the right set of primitives by predicting solutions for test data that are “like” those that worked for training data. Tulsiani *et al.* parse 3D shapes into cuboids, trained without ground truth segmentations [49]. Zou *et al.* parse with a recurrent architecture [57]. Liu *et al.* produce detailed reconstructions of objects in indoor scenes, but do not attempt parsimonious abstraction [32]. Worryingly, 3D reconstruction networks might rely on object semantics [48]. Deng *et al.* (CVXNet) represent objects as a union of convexes, again training without ground truth segmentations [7]. An early variant of CVXNet can recover 3D representations of poses from single images, with reasonable parses into parts [8]. Meshes can be decomposed into near convex primitives, by a form of search [54]. Part decompositions have attractive editability [18]. Regression methods face some difficulty producing different numbers of primitives per scene (CVXNet uses a fixed number; [49] predicts the probability a primitive is present; one also might use Gumbel softmax [22]). Primitives that have been explored include: cuboids [5, 12, 33, 49, 42, 45, 47, 25]; superquadrics [2, 21, 38]; planes [6, 30]; and generalized cylinders [36, 58, 29]. There is a recent review in [11].

Neural Parts [37] decomposes an object given by an image into a set of non-convex shapes. CAPRI-Net [56] decomposes 3D objects given as point clouds or voxel grids into assemblies of quadric surfaces. DeepCAD [55] decomposes an object into a sequence of commands describing a CAD model, but requires appropriately annotated data for training. Point2Cyl [50] is similar, but predicts the 2D shapes in form of an SDF. Notably, [56, 55, 50] also utilise CSG with negative primitives or parts but, unlike our work, focus on CAD models of single objects instead of complex real-world scenes.

Hoiem *et al* parse outdoor scenes into vertical and horizontal surfaces [19, 20]; Gupta *et al* demonstrate a parse into blocks [13]. Indoor scenes can be parsed into: a cuboid [15, 52, 53]; beds and some furniture as boxes [16]; free space [17]; and plane layouts [46, 31]. If RGBD is available, one can recover layout in detail [59]. Patch-like primitives can be imputed from data [10]. Jiang demonstrates parsing RGBD images into primitives by solving a 0-1 quadratic program [23]. Like that work, we evaluate segmentation by primitives (see [23], p. 12), but we use original NYUv2 labels instead of the drastically simplified ones in the prior work. Also, our primitives are truly convex. Monnier *et al* and Alaniz *et al* decompose scenes into sets of superquadrics using differentiable rendering, which requires calibrated multi-view images as input [34, 1]. Most similar to our work is that of Kluger *et al*, who identify cuboids sequentially with a RANSAC-like [9, 26, 28] greedy algorithm [25, 27].

The success of a descent method depends critically on the start point, typically dealt with using greedy algorithms (rooted in [9]; note the prevalence of RANSAC in a recent review [24]); randomized search [40, 14]; or multiple starts. Regression methods must minimize loss over all training data, so at inference time do not necessarily produce the best representation for the particular scene. The prediction is biased by the need to get other scenes right, too. To manage this difficulty, we use a mixed reconstruction strategy – first, predict primitives using a network, then polish using descent.

3 Method

Our work is based on the architecture and losses of [52] and maintains its basic inference procedure:

1. Predict initial convex parameters from an RGBD image via a convolutional neural network.
2. Refine the fit by directly optimizing convex parameters against the training losses.

Unlike [52], we employ an ensemble of multiple networks that predict varying numbers of convexes, and select the prediction which yields the lowest error after refinement (Sec. 3.1). This allows us to abandon the pruning heuristic used by [52] to control the number of convexes for each scene. We furthermore introduce *negative* boolean primitives for scene decomposition (Sec. 3.2). As visualised in Fig. 3, boolean primitives allow for a more parsimonious description of complex geometry. An additional loss, annealing schedule and data augmentation yield further accuracy gains (Sec. 3.3). Fig. 2 provides an overview of our inference pipeline.

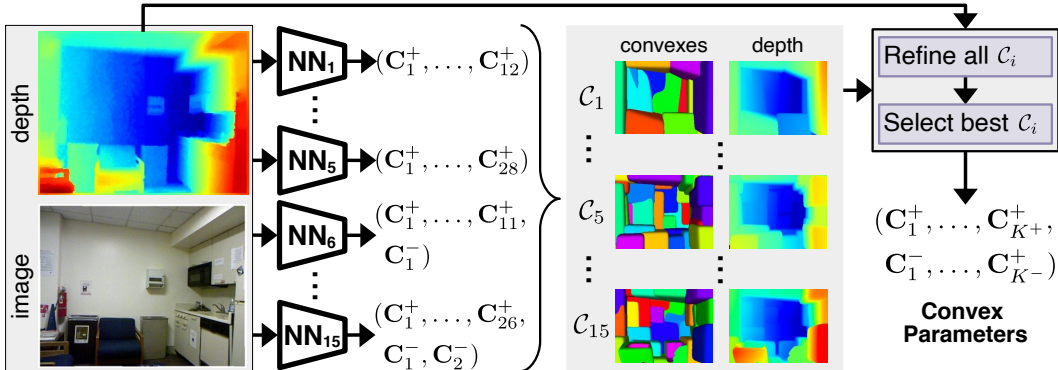


Figure 2: **Inference Overview:** We feed an RGBD image into an ensemble of independently trained convolutional neural networks. Each network predicts the parameters of a set of convexes \mathcal{C}_i . The number of convexes predicted by each network varies between 12 and 28, with up to two of them being negative. We refine each set of convexes by minimizing the training loss w.r.t. the input depth map. Our final decomposition consists of the set of refined convexes \mathcal{C}_i which yields the lowest absolute relative depth error.

3.1 Ensembling

We remark that much of the literature on primitive decomposition fits a fixed number of primitives [7]. Other work starts from a fixed number of primitives and removes excess primitives according to a greedy algorithm [52]. The problem with these approaches is that it is difficult to know a priori what initial settings are best for a given test image. A solution we employ in this work is ensembling the prediction from multiple networks, and selecting the best one. We train networks with different numbers of primitives to construct an ensemble; an even richer ensemble can be constructed by varying weights for some of the training losses, which can substantially effect the behavior of the resulting decomposition even when the number of primitives is the same. To temper the compute requirements, we focus on varying the number of initial primitives and show that this ensemble is sufficient to boost final quality.

For a given test image, we can evaluate by running each test image on each network, evaluating the generated primitive depth map against an inferred or GT depth, and use the best network for subsequent refinement. In practice, we observed refine-then-choose to perform better, whereby we refine each method first then choose the one with the best error metrics. Even though this involves more compute, the quality gains are substantial (see Table 2).

3.2 Boolean primitives

A traditional collection of primitives is represented by an indicator function $O : \mathbb{R} \rightarrow [0, 1]$, with $O(x) = 0$ indicating free space, and $O(x) = 1$ indicating a query point $x \in \mathbb{R}^3$ is inside the volume. When introducing negative primitives, the final indicator can be composed of a CSG operation between the union of positive primitives and union of negative primitives. Let $O^+(x)$ be the indicator of positive primitives only, and $O^-(x)$ be the indicator of negative primitives only. The final indicator for our representation is simply

$$O(x) = \text{ReLU}(O^+(x) - O^-(x)) \quad (1)$$

Our modified representation allows re-using the existing sample loss, unique parametrization loss, and manhattan world loss [7, 52] for both $O^+(x)$ and $O^-(x)$. However, for negative primitives only, we must modify the samples on which the overlap loss, guidance loss, and localization loss are applied. During each training iteration, we select samples for which the ground truth label for a point is *outside*, $x = 0$, but the indicator function is positive, $O(x) = 1$. Thus if a negative primitive moves to such a sample, its classification will become $O(x) = 0$, matching ground truth.

Our early experimentation showed that we are better off pretraining with positive primitives only, and then introducing negative primitives midway through training. Conceptually, this procedure allows

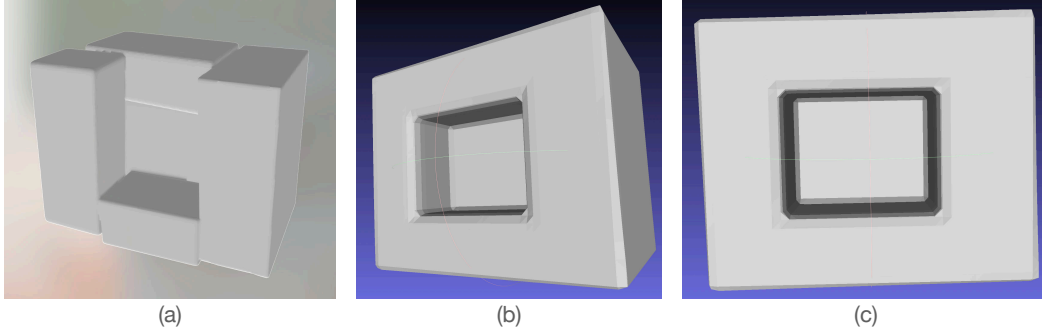


Figure 3: **Boolean primitives are parameter-efficient.** Representing a simple box with a hole can be challenging even with several traditional primitives, as shown in (a), where five primitives get stuck in a local minimum. In contrast, two primitives - one positive and one negative - can represent the geometry successfully because of the enriched vocabulary of operations. Two views are shown in (b) and (c).

positive primitives to explain the scene at a high level, and then negative primitives to subsequently improve the representation.

3.3 Performance improvements

Biasing sample loss The primary loss for training a convex decomposition network is

$$L_{approx} = \mathbb{E}_{x \sim \mathbb{R}^3} \|\hat{O}(x) - O(x)\|^2. \quad (2)$$

We postulate that negative primitives would be most useful in regions that the positive primitives over-explain certain geometry, i.e. they explain more inside samples correctly than outside samples. In effect, if the positive primitives are “too big”, then negative primitives will help the network carve away unnecessary geometry. In other words, there will be more useful regions that negative primitives can exist. We can achieve this bias by simply introducing an additional sample loss but only apply it to points where the GT label is inside, $O(x) = 1$

$$L_{inside} = \mathbb{E}_{x \sim \mathbb{R}^3} \|\hat{O}(x) - 1\|^2. \quad (3)$$

We weight L_{inside} by 0.1, and ablate that choice in Table 4.

Annealing loss weights Further, we found more stable training by annealing the weight of the overlap loss and alignment loss, starting from 0 at the beginning of training, up to the target weight midway through training. We preserve the annealing of the surface sample weight, whereby early in training free space samples are prioritized in the losses, and by midway of training, all samples have an equal weight. All these performance improvements are intended to aid the network in predicting high-level geometric structure of the scene early in training, then getting the details right towards the end.

Data augmentation Prior art did not successfully implement data augmentations in the form of vertical and horizontal flips. A correct implementation needs to take into account the effect of camera calibration parameters on the point cloud. We do so here and in practice, we observe substantial improvements across the board – see Table 5.

Augmentations are especially valuable given that the NYUv2 dataset is relatively small - though clearly sufficient for getting good results. Our procedure uses the standard 795/654 train/test NYUv2 split [35]. We use this dataset primarily to maintain consistency with existing evaluation metrics. We do not consider the volume loss or segmentation loss from [52] in our experimentation, as they were shown to have an approx. neutral effect in prior work.

We implement our procedure in tensorflow and train all networks with Adam optimizer, learning rate 1.5×10^{-4} , batch size 48, for 12000 iterations, requiring 2.5 hours on a single A40 GPU. Our method is RGBD input. Refining a single test image requires ~ 55 seconds for each network in an ensemble. Computing all results in Sec. 4 required approximately 800 GPU hours in total, including preliminary experiments.

Ensemble	K^{total}	K^-	AbsRel ↓	Normals _{mean} ↓	Normals _{median} ↓	Seg _{acc} ↑
No	12	0	<u>0.130</u>	38.219	<u>34.285</u>	0.588
No	12	1	0.132	38.719	34.771	0.585
No	12	2	0.131	39.289	35.018	<u>0.590</u>
No	16	0	<u>0.126</u>	38.404	35.177	<u>0.608</u>
No	16	1	0.128	<u>38.332</u>	<u>34.460</u>	0.605
No	16	2	0.131	38.776	34.933	0.598
No	20	0	<u>0.125</u>	41.606	36.726	<u>0.635</u>
No	20	1	0.130	39.423	35.549	0.619
No	20	2	0.128	<u>38.857</u>	<u>35.405</u>	0.621
No	24	0	<u>0.120</u>	38.930	35.744	<u>0.647</u>
No	24	1	0.123	39.250	35.255	0.640
No	24	2	0.124	<u>38.670</u>	<u>34.513</u>	0.639
No	28	0	0.127	<u>38.717</u>	35.071	0.637
No	28	1	<u>0.124</u>	39.769	35.417	0.647
No	28	2	0.126	38.864	<u>34.856</u>	0.643
pos	21.1	0	0.111	38.861	34.839	0.638
pos + neg	21.9	0.89	0.106	<u>38.535</u>	34.265	<u>0.639</u>

Table 1: **Evaluation without refinement:** Regressors with a fixed number of primitives tend to work better when negative primitives are introduced, but negative primitives are not in themselves a major improvement. For some scenes, the fitting difficulties created by the negative primitives outweighs the improvements, but on average there tends to be some advantage. Each row is a regressor; K^{total} gives the number of primitives; K^- the number of negative primitives. Metrics are standard for depth, normals and segmentation.

4 Experiments

We perform extensive quantitative and qualitative evaluation of our method. To do so, we use established evaluation procedures on the depth, normals, and segmentation inferred from the generated primitives. **Ensembling regression alone is beneficial.** In Table 1, we present several networks with different numbers of positive and negative primitives. We do not apply refinement at test time. Individually, each procedure performs quite well across a range of initial primitives. In some cases, introducing negative primitives helps on average (we test $K^- \in [0, 1, 2]$). When we ensemble the five networks without negative primitives, we get substantially better error metrics, particularly as measured by AbsRel of the depth map. To select the best method, we simply compare the depth of generated primitives against GT. **Ensembling with negative primitives boosts quality.** Further, when we enrich the vocabulary of operations with negative primitives, all error metrics get better across the board (**pos+neg**).

Refinement improves all methods. In Table 2, we apply our refinement procedure on all test images using the GT depth map. Consistent with previous work, refining is essential to getting the best results. Observe how all error metrics, particularly AbsRel, get better with refinement, comparing Table 2 against Table 1. In particular, the negative primitives we introduced get better with refinement. While we get strong results across all numbers of primitives, the introduction of negative primitives only occasionally helps on average, in some cases slightly hurting metrics, which indicates that our test scenes are quite diverse and different settings are optimal for each scene. **Refine-then-select performs better than select-then-refine.** When we ensemble the five positive-only networks, rows **pos**, all error metrics get better than any method alone. However, the fact that we get better numbers when we select after refining indicates that this is an extremely difficult fitting problem whereby what appears to be the best start point may not necessarily yield the best endpoint. When comparing ensembles with negative primitives (**pos+neg**), we again observe that we are better off refining then selecting. Further, on average the network picks 0.80 negative primitives in our best ensemble - which means they are genuinely helpful on some scenes. In Fig 4 we present histograms showing how many total and negative primitives were chosen on our test set. In practice, (**left**) our procedure

Ensemble	Refine	K^{total}	K^-	AbsRel ↓	Normals _{mean} ↓	Normals _{median} ↓	Seg _{acc} ↑
No (V. et al [52])	Yes	13.9	0	0.098	37.355	32.395	0.618
No (V. et al [52])	Yes	15.7	0	0.096	37.355	32.700	0.630
No	Yes	12	0	<u>0.086</u>	<u>35.646</u>	<u>30.851</u>	<u>0.611</u>
No	Yes	12	1	0.090	36.211	31.401	0.600
No	Yes	12	2	0.088	36.383	31.386	0.607
No	Yes	16	0	<u>0.079</u>	<u>35.412</u>	31.099	<u>0.632</u>
No	Yes	16	1	0.083	35.762	<u>31.031</u>	0.626
No	Yes	16	2	0.087	36.138	31.792	0.613
No	Yes	20	0	<u>0.078</u>	37.520	31.771	<u>0.657</u>
No	Yes	20	1	0.083	36.416	31.680	0.637
No	Yes	20	2	0.081	<u>35.831</u>	<u>31.535</u>	0.639
No	Yes	24	0	<u>0.074</u>	35.472	31.511	<u>0.667</u>
No	Yes	24	1	<u>0.074</u>	<u>35.334</u>	<u>30.441</u>	0.662
No	Yes	24	2	0.075	35.378	30.539	0.661
No	Yes	28	0	<u>0.073</u>	35.050	<u>30.403</u>	<u>0.672</u>
No	Yes	28	1	<u>0.073</u>	35.942	30.825	0.670
No	Yes	28	2	0.077	35.321	30.501	0.667
pos	S→R	21.1	0	<u>0.076</u>	35.721	30.932	<u>0.657</u>
pos + neg	S→R	21.9	0.89	<u>0.076</u>	<u>35.677</u>	<u>30.836</u>	0.655
pos	R→S	24.41	0	0.066	35.138	30.149	0.662
pos + neg	R→S	24.83	0.80	0.064	<u>35.085</u>	29.950	0.676

Table 2: **Evaluation with refinement:** Refinement – polishing the convexes predicted by the regressor against the depth – improves fits significantly (cf. top block with Table 1), but the best strategy by far is to ensemble (bottom block). Ensembles with negative primitives available do best. Generally, refine-then-select (R→S) is significantly better than select-then-refine (S→R), likely because the fitting problem is extremely hard, so the start point for refining is a poor guide to how well the refinement will proceed. In the bottom block, the K^- indicates the average number of negative primitives used per image, suggesting the best fit for a significant fraction of images has one or more negative primitives. First two rows: **Even with fewer primitives, any individual network performs better than prior art.**

is able to handle larger numbers of primitives better than prior work, observing that more primitives is generally better, and **right**, negative primitives can be quite helpful, noting that they are selected from the ensemble about half the time.

A biased sampling loss should be part of the ensemble. We ablate our decision to bias the sampling loss to favor classifying “inside” points correctly via L_{inside} . In Table 4, we test $w_{inside} \in [0.0, 0.1, 0.2, 0.4]$ with $K^- = 1$. This loss is clearly helpful across all numbers we tried. Yet, when more positive primitives are present, $K^{total} = 20$, the loss hurts quality. We thus let $w_{inside} = 0.1$ in our experimentation as a reasonable mid-ground.

Data augmentation yields more accurate decompositions. As Table 5 shows, augmenting RGBD input data with horizontal and vertical flips during training reduces the AbsRel depth error and increases the segmentation accuracy measurably, albeit with a marginal penalty w.r.t. normal accuracy.

Any individual network we train beats baselines. Without ensembling, with or without negative primitives, our method beats all baselines on nearly every metric - see Tables 2, 3.

Our combination of improvements strongly outperforms existing baselines. We can evaluate our approach using the occlusion-aware distance metric from [25]. Our ensembles with positive and positive+negative primitives strongly outcompete existing baselines.

	AUC@50↑	AUC@20↑	AUC@10↑	AUC@5↑	mean _{cm} ↓	median _{cm} ↓
Vavilala <i>et al.</i> [52]	86.9	72.5	56.5	38.2	26.6	10.1
Kluger <i>et al.</i> [25]	77.2	62.7	49.1	34.3	20.8	-
12/0	88.4	75.7	59.6	39.8	24.2	8.9
16/0	89.3	77.7	62.2	42.3	22.8	8.2
20/0	89.2	78.2	63.4	44.2	22.9	7.9
24/0	90.1	79.6	64.2	43.3	21.4	7.6
28/0	90.2	80.7	66.9	47.1	21.3	7.0
12/1	87.5	74.2	58.3	39.3	25.5	9.3
16/1	88.5	76.7	61.5	42.2	24.1	8.4
20/1	88.3	76.4	61.0	42.1	24.7	8.3
24/1	89.9	79.8	65.8	46.7	21.6	7.1
28/1	89.9	79.9	66.2	47.4	21.6	7.0
12/2	87.4	74.7	59.2	40.5	25.7	9.2
16/2	87.8	75.3	59.1	39.6	25.6	9.2
20/2	88.7	77.4	62.0	42.1	24.1	8.4
24/2	89.8	79.9	65.8	46.3	22.1	7.2
28/2	89.3	79.7	66.1	47.0	22.7	7.2
Ours (pos)	91.2	81.5	67.1	47.3	19.3	6.79
Ours (pos + neg)	91.5	82.0	68.0	48.4	18.8	6.58

Table 3: **Baseline comparisons:** Ensembling strongly outperforms two recent SOTA methods, using the metrics reported by [25], and using negative primitives in the ensemble produces further improvements. We ensemble with refine-then-select, and show results with only positive primitives present (**Ours (pos)**, five networks, $K^{total} \in [12, 16, 20, 24, 28]$), as well as with positive and negative primitives (**Ours (pos+neg)**, 15 networks, $K^- \in [0, 1, 2]$). Our ensembles significantly outperform existing work. Further, we present results on the fifteen methods we trained, where K^{total}/K^- is shown. Even without ensembling, any individual method we trained performs better than the baselines across every metric except mean_{cm}.

w_{inside}	K^{total}	K^-	AbsRel ↓	Normals _{mean} ↓	Normals _{median} ↓	Seg _{acc} ↑
0.0	12	1	0.122	37.693	33.136	0.556
0.1	12	1	0.090	36.211	31.401	0.600
0.2	12	1	0.093	36.292	31.736	0.594
0.4	12	1	0.097	36.424	31.482	0.607
0.0	20	1	0.080	35.707	31.301	0.651
0.1	20	1	0.083	36.416	31.680	0.637
0.2	20	1	0.086	36.521	31.620	0.637
0.4	20	1	0.090	36.388	32.470	0.642

Table 4: **Biased sampling loss:** Weighting errors on inside samples higher than those on outside samples helps, particularly in the regime where there is a negative primitive and there are few positive primitives. This is likely a form of crude boosting effect, that forces the negative to “cut out” incorrectly classified inside samples. $w_{inside} = 0$ is no bias; increasing values are more biased.

Augment	K^{total}	K^-	AbsRel ↓	Normals _{mean} ↓	Normals _{median} ↓	Seg _{acc} ↑
Yes	24	0	0.074	35.472	31.511	0.667
No	24	0	0.080	35.414	30.773	0.652

Table 5: **Data augmentation:** Unlike prior work [52], we utilize data augmentation of 3D samples in the form of random vertical and horizontal flips during training. This yields better decompositions as measured by AbsRel depth error and segmentation accuracy. We consider the slightly worse normals an acceptable trade-off and they are worth continued investigation.

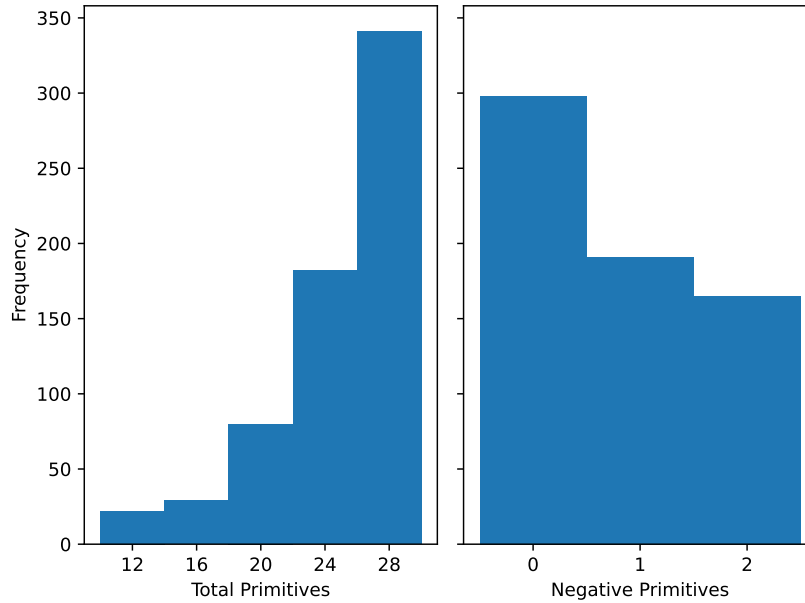


Figure 4: There are a wide range of active participants in the ensemble. This figure shows the frequency with which ensemble members are chosen by refine-then-select for 654 test scenes, broken out by number of positive primitives and number of negative primitives. Note how often regressors with large numbers of positive primitives are chosen; and that negative primitives are used frequently.

5 Discussion

The key goal of primitive representations since the 1960s has been to demonstrate representations that can (a) be computed from data and (b) genuinely simplify reasoning tasks. We have demonstrated a method that can produce accurate fits of multiple convex primitives, some “negative”, to complex indoor scenes represented in RGBD images. Our method really can be computed from data, and in accuracy significantly outperforms SOTA.

Limitations The method requires ensembling a number of regressors, with consequent costs in training and inference time. While we can evaluate accuracy, it is difficult to usefully assess the extent to which the method is parsimonious, apart from looking at the relatively small number of primitives used. We have shown partial progress on simplifying reasoning tasks (the segmentation implied by the primitives is fair, but not competitive with the best semantic segmenters). In general, demonstrating that primitives are useful remains open, as it has since the 1960s.

References

- [1] Stephan Alaniz, Massimiliano Mancini, and Zeynep Akata. Iterative superquadric recomposition of 3d objects from multiple views. In *Proceedings of the IEEE/CVF International Conference on Computer Vision*, pages 18013–18023, 2023.
- [2] Barr. Superquadrics and angle-preserving transformations. *IEEE Computer Graphics and Applications*, 1:11–23, 1981.
- [3] I Biederman. Recognition by components : A theory of human image understanding. *Psychological Review*, (94):115–147, 1987.
- [4] TO Binford. Visual perception by computer. In *IEEE Conf. on Systems and Controls*, 1971.
- [5] Stéphane Calderon and Tamy Boubekeur. Bounding proxies for shape approximation. *ACM Transactions on Graphics (TOG)*, 36:1 – 13, 2017.
- [6] Zhiqin Chen, Andrea Tagliasacchi, and Hao Zhang. Bsp-net: Generating compact meshes via binary space partitioning. *2020 IEEE/CVF Conference on Computer Vision and Pattern Recognition (CVPR)*, pages 42–51, 2019.

- [7] Boyang Deng, Kyle Genova, Soroosh Yazdani, Sofien Bouaziz, Geoffrey Hinton, and Andrea Tagliasacchi. Cvxnet: Learnable convex decomposition. June 2020.
- [8] Boyang Deng, Simon Kornblith, and Geoffrey Hinton. Cerberus: A multi-headed derenderer. In *Workshop on 3D Scene Understanding*, 2019.
- [9] M. A. Fischler and R. C. Bolles. Random sample consensus: A paradigm for model fitting with applications to image analysis and automated cartography. *Comm. ACM.*, 24(6):381–395, 1981.
- [10] David F. Fouhey, Abhinav Gupta, and Martial Hebert. Data-driven 3D primitives for single image understanding. In *ICCV*, 2013.
- [11] K. Fu, J. Peng, and Q. He et al. Single image 3d object reconstruction based on deep learning: A review. *Multimed Tools Appl.*, 80:463–498, 2021.
- [12] Matheus Gadelha, Giorgio Gori, Duygu Ceylan, Radomír Mech, Nathan A. Carr, Tamy Boubekeur, Rui Wang, and Subhansu Maji. Learning generative models of shape handles. *2020 IEEE/CVF Conference on Computer Vision and Pattern Recognition (CVPR)*, pages 399–408, 2020.
- [13] Abhinav Gupta, Alexei A. Efros, and Martial Hebert. Blocks world revisited: Image understanding using qualitative geometry and mechanics. In *ECCV*, 2010.
- [14] Shreyas Hampali, Sinisa Stekovic, Sayan Deb Sarkar, Chetan Srinivasa Kumar, Friedrich Fraundorfer, and Vincent Lepetit. Monte carlo scene search for 3d scene understanding. *2021 IEEE/CVF Conference on Computer Vision and Pattern Recognition (CVPR)*, pages 13799–13808, 2021.
- [15] V. Hedau, D. Hoiem, and D. Forsyth. Recovering the Spatial Layout of Cluttered Rooms. In *Proc. ICCV*, 2009.
- [16] Varsha Hedau, Derek Hoiem, and David Forsyth. Thinking Inside the Box: Using Appearance Models and Context Based on Room Geometry. In *Proc. ECCV*, 2010.
- [17] V. Hedau, D. Hoiem, and D. Forsyth. Recovering Free Space of Indoor Scenes from a Single Image. In *Proc. CVPR*, 2012.
- [18] A. Hertz, O. Perel, O. Sorkine-Hornung, and D. Cohen-Or. Spaghetti: editing implicit shapes through part aware generation. *ACM Transactions on Graphics*, 41(4):1–20, 2022.
- [19] Derek Hoiem, Alexei A. Efros, and Martial Hebert. Automatic photo pop-up. *ACM Transactions on Graphics / SIGGRAPH*, 24(3), Aug. 2005.
- [20] D. Hoiem, A. A. Efros, and M. Hebert. Recovering surface layout from an image. *IJCV*, 2007.
- [21] Aleš Jaklič, Aleš Leonardis, and Franc Solina. Segmentation and recovery of superquadrics. In *Computational Imaging and Vision*, 2000.
- [22] Eric Jang, Shixiang Gu, and Ben Poole. Categorical reparameterization with gumbel-softmax. In *International Conference on Learning Representations*, 2017.
- [23] Hao Jiang. Finding approximate convex shapes in rgbd images. In *European Conference on Computer Vision*, pages 582–596. Springer, 2014.
- [24] Zhizhong Kang, Juntao Yang, Zhou Yang, and Sai Cheng. A review of techniques for 3d reconstruction of indoor environments. *ISPRS Int. J. Geo Inf.*, 9:330, 2020.
- [25] Florian Kluger, Hanno Ackermann, Eric Brachmann, Michael Ying Yang, and Bodo Rosenhahn. Cuboids revisited: Learning robust 3d shape fitting to single rgb images. In *Proceedings of the IEEE Conference on Computer Vision and Pattern Recognition (CVPR)*, 2021.
- [26] Florian Kluger, Eric Brachmann, Hanno Ackermann, Carsten Rother, Michael Ying Yang, and Bodo Rosenhahn. CONSAC: Robust Multi-Model Fitting by Conditional Sample Consensus. In *CVPR*, 2020.
- [27] Florian Kluger, Eric Brachmann, Michael Ying Yang, and Bodo Rosenhahn. Robust shape fitting for 3d scene abstraction. *IEEE Transactions on Pattern Analysis and Machine Intelligence*, 2024.
- [28] Florian Kluger and Bodo Rosenhahn. PARSAC: Accelerating Robust Multi-Model Fitting with Parallel Sample Consensus. In *AAAI*, 2024.
- [29] Lingxiao Li, Minhyuk Sung, Anastasia Dubrovina, L. Yi, and Leonidas J. Guibas. Supervised fitting of geometric primitives to 3d point clouds. *2019 IEEE/CVF Conference on Computer Vision and Pattern Recognition (CVPR)*, pages 2647–2655, 2018.
- [30] Chen Liu, Kihwan Kim, Jinwei Gu, Yasutaka Furukawa, and Jan Kautz. PlanerCNN: 3d plane detection and reconstruction from a single image. *2019 IEEE/CVF Conference on Computer Vision and Pattern Recognition (CVPR)*, pages 4445–4454, 2018.
- [31] Chen Liu, Jimei Yang, Duygu Ceylan, Ersin Yumer, and Yasutaka Furukawa. Planenet: Piece-wise planar reconstruction from a single rgb image. In *Proceedings of the IEEE Conference on Computer Vision and Pattern Recognition*, pages 2579–2588, 2018.
- [32] Haolin Liu, Yujian Zheng, Guanying Chen, Shuguang Cui, and Xiaoguang Han. Towards high-fidelity single-view holistic reconstruction of indoor scenes. In *European Conference on Computer Vision*, pages 429–446. Springer, 2022.
- [33] Kaichun Mo, Paul Guerrero, L. Yi, Hao Su, Peter Wonka, Niloy Jyoti Mitra, and Leonidas J. Guibas. Structurenets: Hierarchical graph networks for 3d shape generation. *ACM Trans. Graph.*, 38:242:1–242:19, 2019.

- [34] Tom Monnier, Jake Austin, Angjoo Kanazawa, Alexei Efros, and Mathieu Aubry. Differentiable blocks world: Qualitative 3d decomposition by rendering primitives. *Advances in Neural Information Processing Systems*, 36:5791–5807, 2023.
- [35] Pushmeet Kohli Nathan Silberman, Derek Hoiem and Rob Fergus. Indoor segmentation and support inference from rgb-d images. In *ECCV*, 2012.
- [36] R. Nevatia and T.O. Binford. Description and recognition of complex curved objects. *Artificial Intelligence*, 1977.
- [37] Despoina Paschalidou, Angelos Katharopoulos, Andreas Geiger, and Sanja Fidler. Neural parts: Learning expressive 3d shape abstractions with invertible neural networks. In *CVPR*, 2021.
- [38] Despoina Paschalidou, Ali O. Ulusoy, and Andreas Geiger. Superquadrics revisited: Learning 3d shape parsing beyond cuboids. *2019 IEEE/CVF Conference on Computer Vision and Pattern Recognition (CVPR)*, pages 10336–10345, 2019.
- [39] J. Ponce and M. Hebert. A new method for segmenting 3-d scenes into primitives. In *Proc. 6 ICPR*, 1982.
- [40] Michael Ramamonjisoa, Sinisa Stekovic, and Vincent Lepetit. Monteboxfinder: Detecting and filtering primitives to fit a noisy point cloud. *ArXiv*, abs/2207.14268, 2022.
- [41] René Ranftl, Katrin Lasinger, David Hafner, Konrad Schindler, and Vladlen Koltun. Towards robust monocular depth estimation: Mixing datasets for zero-shot cross-dataset transfer. *IEEE Transactions on Pattern Analysis and Machine Intelligence*, 44(3), 2022.
- [42] Dominic Roberts, Aram Danielyan, Hang Chu, Mani Golparvar Fard, and David A. Forsyth. Lsd-structurenet: Modeling levels of structural detail in 3d part hierarchies. *2021 IEEE/CVF International Conference on Computer Vision (ICCV)*, pages 5816–5825, 2021.
- [43] L. G. Roberts. *Machine Perception of Three-Dimensional Solids*. PhD thesis, MIT, 1963.
- [44] S. Shafer and T. Kanade. The theory of straight homogeneous generalized cylinders. In *Technical Report CS-083-105, Carnegie Mellon University*, 1983.
- [45] Dmitriy Smirnov, Matthew Fisher, Vladimir G. Kim, Richard Zhang, and Justin M. Solomon. Deep parametric shape predictions using distance fields. *2020 IEEE/CVF Conference on Computer Vision and Pattern Recognition (CVPR)*, pages 558–567, 2019.
- [46] Sinisa Stekovic, Shreyas Hampali, Mahdi Rad, Sayan Deb Sarkar, Friedrich Fraundorfer, and Vincent Lepetit. General 3d room layout from a single view by render-and-compare. In *European Conference on Computer Vision*, pages 187–203. Springer, 2020.
- [47] Chun-Yu Sun and Qian-Fang Zou. Learning adaptive hierarchical cuboid abstractions of 3d shape collections. *ACM Transactions on Graphics (TOG)*, 38:1 – 13, 2019.
- [48] Maxim Tatarchenko, Stephan R. Richter, René Ranftl, Zhuwen Li, Vladlen Koltun, and Thomas Brox. What do single-view 3d reconstruction networks learn? *2019 IEEE/CVF Conference on Computer Vision and Pattern Recognition (CVPR)*, pages 3400–3409, 2019.
- [49] Shubham Tulsiani, Hao Su, Leonidas J. Guibas, Alexei A. Efros, and Jitendra Malik. Learning shape abstractions by assembling volumetric primitives. In *Computer Vision and Pattern Recognition (CVPR)*, 2017.
- [50] Mikaela Angelina Uy, Yen-Yu Chang, Minhyuk Sung, Purvi Goel, Joseph G Lambourne, Tolga Birdal, and Leonidas J Guibas. Point2cyl: Reverse engineering 3d objects from point clouds to extrusion cylinders. In *CVPR*, 2022.
- [51] A. van den Hengel, C. Russell, A. Dick, J. Bastian, L. Fleming D. Poo-ley, and L. Agapito. Part-based modelling of compound scenes from images. In *CVPR*, 2015.
- [52] Vaibhav Vavilala and David Forsyth. Convex decomposition of indoor scenes. In *Proceedings of the IEEE/CVF International Conference on Computer Vision (ICCV)*, pages 9176–9186, October 2023.
- [53] Vaibhav Vavilala, Seemantdar Jain, Rahul Vasanth, Anand Bhattad, and David Forsyth. Blocks2world: Controlling realistic scenes with editable primitives, 2023.
- [54] X. Wei, M. Liu, Z. Ling, and H. Su. Approximate convex decomposition for 3d meshes with collision-aware concavity and tree search. *ACM Transactions on Graphics*, 41(4), 2022.
- [55] Rundi Wu, Chang Xiao, and Changxi Zheng. Deepcad: A deep generative network for computer-aided design models. In *ICCV*, 2021.
- [56] Fenggen Yu, Zhiqin Chen, Manyi Li, Aditya Sanghi, Hooman Shayani, Ali Mahdavi-Amiri, and Hao Zhang. Capri-net: Learning compact cad shapes with adaptive primitive assembly. In *Proceedings of the IEEE/CVF Conference on Computer Vision and Pattern Recognition*, pages 11768–11778, 2022.
- [57] Chuhan Zou, Alex Colburn, Qi Shan, and Derek Hoiem. Layoutnet: Reconstructing the 3d room layout from a single rgb image. In *Proceedings of the IEEE Conference on Computer Vision and Pattern Recognition (CVPR)*, June 2018.
- [58] Chuhan Zou, Ersin Yumer, Jimei Yang, Duygu Ceylan, and Derek Hoiem. 3d-prnn: Generating shape primitives with recurrent neural networks. *2017 IEEE International Conference on Computer Vision (ICCV)*, pages 900–909, 2017.
- [59] Chuhan Zou, Ersin Yumer, Jimei Yang, Duygu Ceylan, and Derek Hoiem. 3d-prnn: Generating shape primitives with recurrent neural networks. In *Proceedings of the IEEE International Conference on Computer Vision (ICCV)*, Oct 2017.

6 Appendix / supplemental material

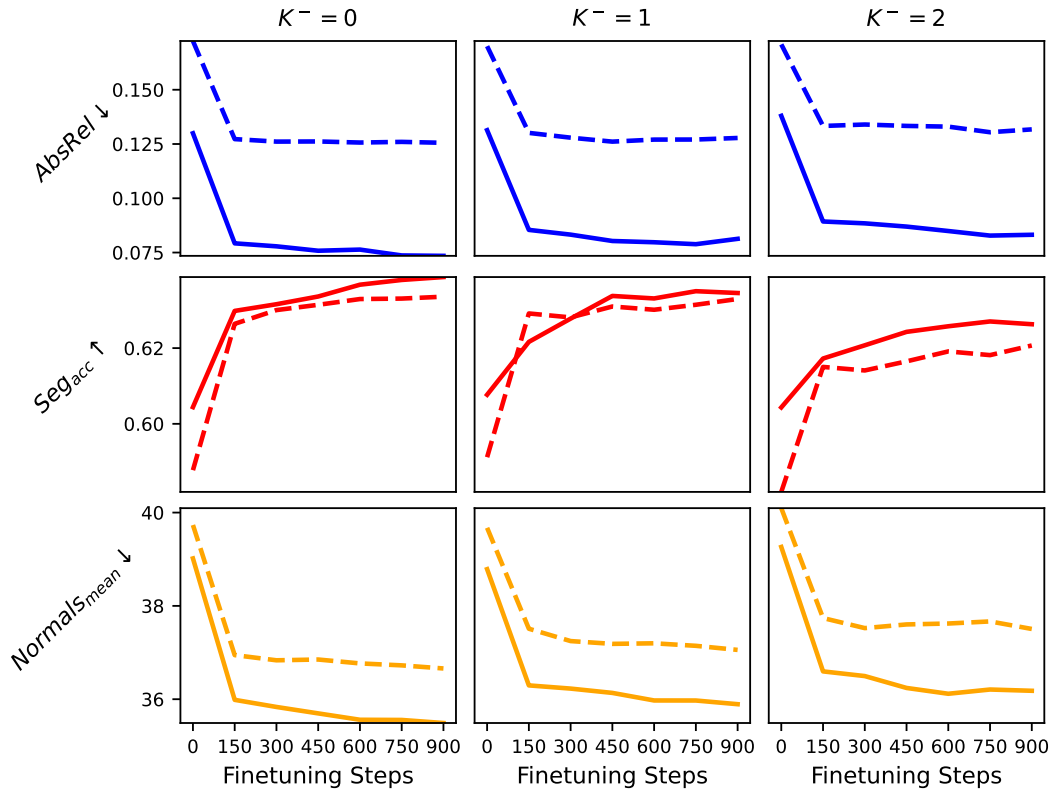


Figure 5: **Ablation on number of finetuning steps.** Polishing the prediction from regression is essential to obtaining good results. This is true both when GT depth is available (**solid line**) or depth must be inferred from RGB (**dashed line**). A different error metric is shown in each row: AbsRel, Segmentation accuracy, and mean normal error (in degrees). Even when introducing negative primitives (**columns 2 and 3**), polishing helps significantly. In this work, we perform quantitative evaluation with 300 finetuning steps wherever we do perform polishing, a reasonable tradeoff between quality and speed. In this figure, $K^{total} = 16$, and we evaluate on 80 random test images.

Ensemble	Refine	K^{total}	K^-	AbsRel ↓	Normals _{mean} ↓	Normals _{median} ↓	Seg _{acc} ↑
No (V. et al [52])	Yes	14.4	0	0.144	38.235	33.621	0.615
No	Yes	12	0	0.1437	<u>36.440</u>	<u>32.491</u>	0.588
No	Yes	12	1	0.1375	37.288	32.765	0.597
No	Yes	12	2	<u>0.1351</u>	37.285	32.606	<u>0.607</u>
No	Yes	16	0	0.1384	<u>36.706</u>	<u>32.369</u>	0.620
No	Yes	16	1	<u>0.1340</u>	36.858	32.411	<u>0.627</u>
No	Yes	16	2	0.1365	37.120	32.871	0.611
No	Yes	20	0	<u>0.1305</u>	37.893	<u>32.814</u>	<u>0.656</u>
No	Yes	20	1	0.1341	37.562	33.089	0.637
No	Yes	20	2	0.1312	<u>37.169</u>	33.083	0.641
No	Yes	24	0	0.1298	<u>36.552</u>	32.261	<u>0.669</u>
No	Yes	24	1	<u>0.1291</u>	36.738	<u>32.181</u>	0.662
No	Yes	24	2	0.1296	36.809	32.238	0.660
No	Yes	28	0	0.1300	<u>36.405</u>	<u>32.101</u>	0.672
No	Yes	28	1	<u>0.1288</u>	37.298	32.596	0.667
No	Yes	28	2	0.1298	36.808	32.272	0.668
pos	S→R	23.284	0	0.1300	36.647	32.142	0.659
pos + neg	S→R	22.514	0.786	0.1296	36.765	32.161	0.654
pos	R→S	27.908	0	0.1294	36.395	32.092	0.672
pos + neg	R→S	27.939	1.997	0.1287	36.929	32.396	0.668

Table 6: **Evaluation with inferred depth:** Our procedure still works well even when ground truth depth isn’t available. Without ensembling, any of our fifteen networks with $K^{total} \in [12, 16, 20, 24, 28]$ and $K^- \in [0, 1, 2]$ perform better than prior work [52], even with fewer primitives available. We can ensemble these networks by evaluating the primitive decomposition against an inferred depth map (we use [41]). $S \rightarrow R$ means that we evaluate AbsRel of the primitives generated by the network against the MIDAS depth map across all members of the ensemble, select the best one, then refine that one (using the MIDAS depth map for supervision in the losses). $R \rightarrow S$ means that we refine predictions from all members of the ensemble on a particular test image, then choose the best one as measured by AbsRel against MIDAS. Ensembling generally helps, particularly when we use $R \rightarrow S$. However, introducing negative primitives into the ensemble yields slightly worse normal and segmentation in exchange for better depth. The implication is that effectively fitting negative primitives remains hard.

	AUC@50↑	AUC@20↑	AUC@10↑	AUC@5↑	mean _{cm} ↓	median _{cm} ↓
Vavilala <i>et al.</i> [52]	77.3	47.6	26.8	13.9	40.2	26.2
Kluger <i>et al.</i> [25]	57.0	33.1	18.9	10.0	34.5	-
12/0	77.8	48.1	27.1	13.9	39.4	26.2
16/0	78.8	49.2	27.8	14.4	37.9	25.1
20/0	80.1	50.7	28.7	14.9	36.7	24.1
24/0	80.4	50.8	28.8	15.0	36.2	24.0
28/0	80.3	50.8	28.7	14.8	36.2	24.1
12/1	78.1	48.7	27.5	14.3	39.2	25.7
16/1	79.0	49.8	28.1	14.6	38.4	25.1
20/1	78.9	49.6	28.1	14.6	38.6	24.8
24/1	79.9	50.8	28.9	15.0	37.1	24.2
28/1	79.9	50.7	28.9	15.0	37.2	24.2
12/2	78.6	49.3	27.9	14.5	38.8	24.8
16/2	78.4	49.1	27.9	14.4	39.1	25.5
20/2	79.5	50.1	28.5	14.7	38.0	24.7
24/2	79.9	50.7	28.8	14.9	37.2	24.1
28/2	79.8	50.7	28.9	15.0	37.3	24.1
Ours (pos)	81.1	51.6	29.4	15.3	35.0	23.16
Ours (pos + neg)	81.4	52.3	30.0	15.7	34.5	22.75

Table 7: **Baseline comparisons with inferred depth:** Ensembling strongly outperforms two recent SOTA methods, using the metrics reported by [25], and using negative primitives in the ensemble produces further improvements. Here, we evaluate when GT depth is not available and must be inferred. We ensemble with refine-then-select, and show results with only positive primitives present (**Ours (pos)**, five networks, $K^{total} \in [12, 16, 20, 24, 28]$), as well as with positive and negative primitives (**Ours (pos+neg)**, 15 networks, $K^- \in [0, 1, 2]$). Our ensembles significantly outperform existing work. Further, we present results on the fifteen methods we trained, where K^{total}/K^- is shown. Even without ensembling, any individual method we trained performs better than the baselines across every metric except mean_{cm}.

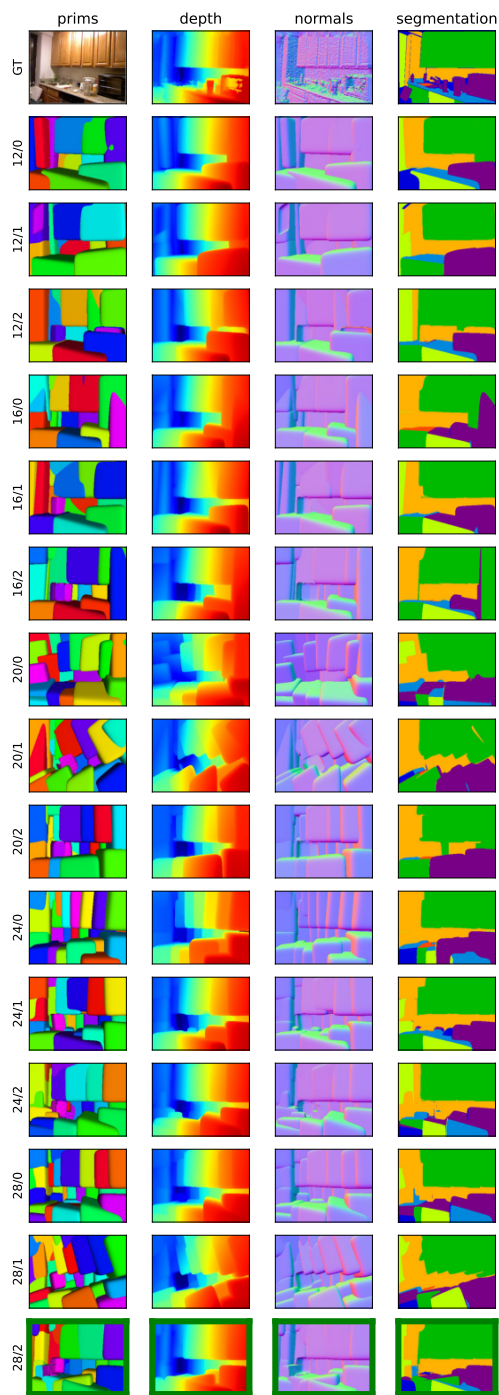


Figure 6: Qualitative evaluation when GT is present, best method chosen by ensemble boxed in green. Row label shows the K^{total}/K^- .

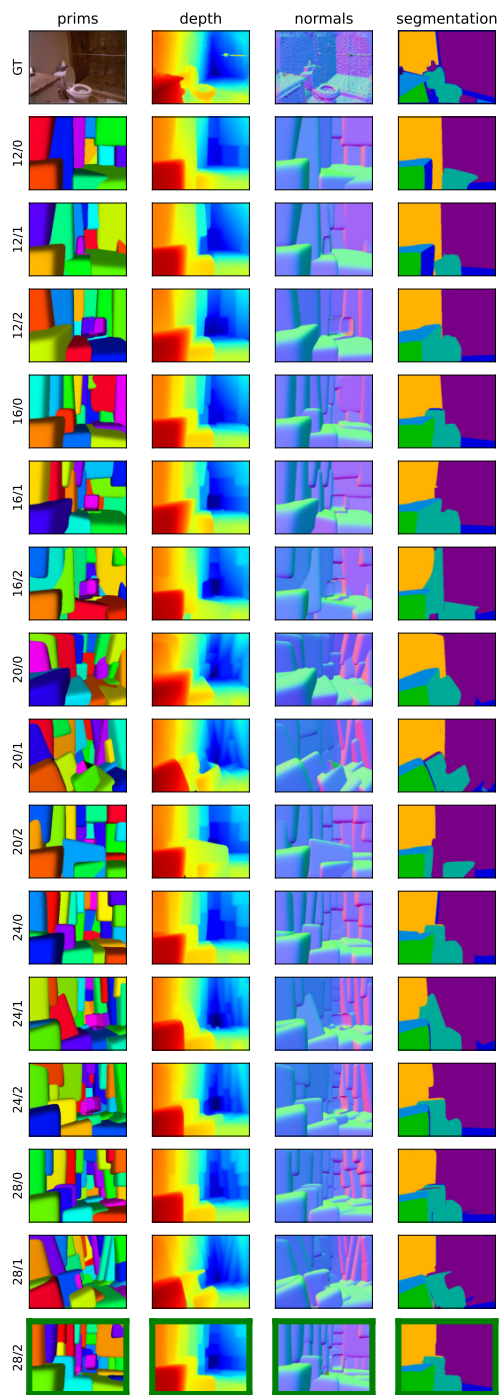


Figure 7: Qualitative evaluation when GT is present, best method chosen by ensemble boxed in green. Row label shows the K^{total}/K^- .

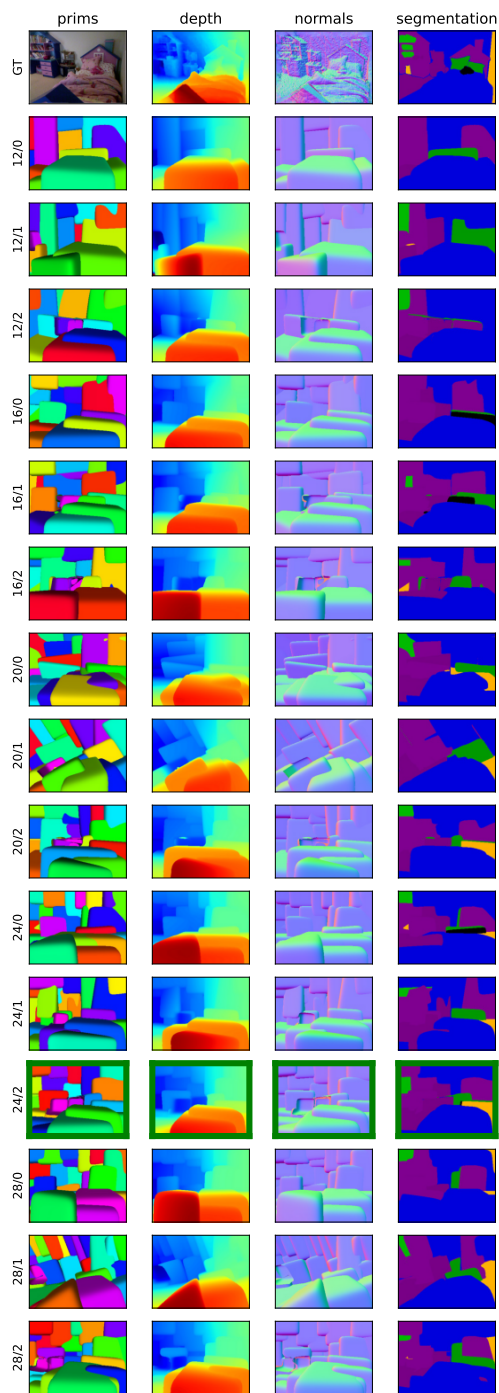


Figure 8: Qualitative evaluation when GT is present, best method chosen by ensemble boxed in green. Row label shows the K^{total}/K^- .

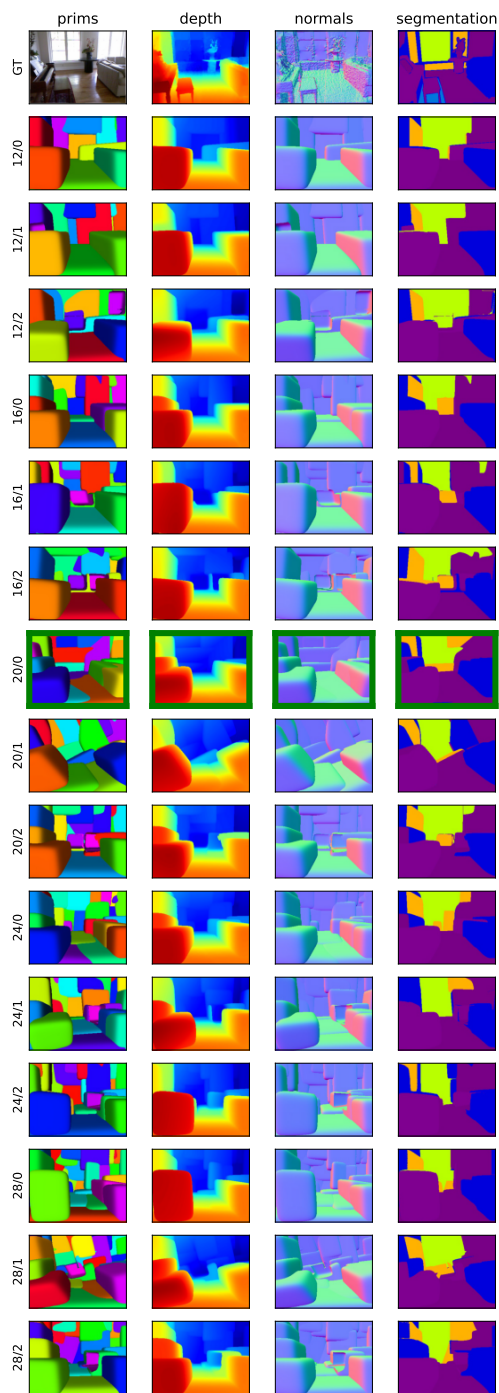


Figure 9: Qualitative evaluation when GT is present, best method chosen by ensemble boxed in green. Row label shows the K^{total}/K^- .